ORIGINAL ARTICLE

Journal Section

Solvation Pressure in Spherical Mesopores: Macroscopic Theory and Molecular Simulations

Alina Emelianova[1] | **Max A. Maximov**[1] | **Gennady Y. Gor**[1]

[1]Otto H. York Department of Chemical and Materials Engineering, New Jersey Institute of Technology, University Heights, Newark, NJ 07102, USA

Correspondence
Gennady Y. Gor
Email: gor@njit.edu

Abstract

Fluids adsorbing in nanoporous solids cause high solvation pressures that deform the solids and affect properties of the fluids themselves. We calculate solvation pressure of nitrogen adsorbed at 77.4 K in spherical silica mesopores using two methods: macroscopic Derjaguin-Broekhoff-de Boer theory and molecular simulations. We show that both approaches give consistent results and the observed pressures increase in smaller pores reaching the order of a hundred megapascals. The results are also typical for the solvation pressure in mesoporous materials, yet noticeably differ from the results for cylindrical pore geometry. Furthermore, we show that the dependence of the solvation pressure at saturation on the reciprocal pore size is linear, and we use this relation for the calculation of the solid-liquid surface energy. The results can be employed for the prediction of the solvation pressure and the adsorption-induced deformation in the material with spherical pore geometry.

Keywords: Adsorption/gas, Computer simulations (MC and MD), Capillary condensation, Adsorption-induced deformation

Note:

This is the peer reviewed version of the following article: Emelianova, A.; Maximov, M. A.; Gor, G. Y. "Solvation Pressure in Spherical Mesopores: Macroscopic Theory and Molecular Simulations" *AIChE J.* 2021, e16542, which has been published in final form at DOI: 10.1002/aic.16542. This article may be used for non-commercial purposes in accordance with Wiley Terms and Conditions for Use of Self-Archived Versions.

INTRODUCTION

Adsorption of fluids in porous structure takes place due to the intermolecular interactions between solid surface and adsorbate. The same forces result in the appearance of high solvation pressure in the pores and cause the deformation of the material [1]. The high pressure in the pores have additional effects other than mechanical strains, in particular, some of the high-pressure chemical reactions take place in the pores at the moderate gas pressures [2;3], or the compressibility of fluids in pores changes [4;5;6;7]. Some of these effects stimulated a series of work on the molecular simulation of high-pressure effects in the pores, published within the last decade by Gubbins group [8;9;10;11;12;13;14;15].

The solvation pressure is introduced as the normal component of the pressure tensor of inhomogeneous fluid confined in a nanopore [16]. The thermodynamic approach for calculating solvation pressure and predicting adsorption-induced deformation based on it, relates it to the derivative of the grand potential of the fluid in a rigid pore [17]. The approach was first applied for the micropores in zeolites (represented as spheres) [17], then generalized to slit- [18;19;20], and wedge-shape [21] micropores in carbons, and cylindrical mesopores [22;23]. The convenience of this approach is that the grand potential can be calculated from any conventional theory for predicting adsorption isotherms. For example, the isotherms can be obtained from grand canonical Monte Carlo (GCMC) simulations or density functional theory (DFT) [24;25].

Although microscopic approaches (GCMC, DFT) have become a standard for predicting adsorption isotherms of simple gases in nanopores and mesopores, in particular, [26] macroscopic approaches are still frequently employed. The popularity of the conservative approaches is not surprising since they provide much more flexibility compared to the DFT method limited to the simplest gases and, even in this case, requiring laborious calculations [25]. Among the macroscopic approaches, the theory of capillary condensation proposed by Derjaguin [27] still remains widely used. Applied by Broekhoff and de Boer for pore size distribution calculations [28;29], this approach is typically referred to as Derjaguin-Broekhoff-de Boer (DBdB) theory. The success of this particular theory is likely due to its simplicity and demonstrated consistency with the DFT approach and with experimental data for nitrogen and argon adsorption in mesoporous silica [30]. DBdB has been recently applied for calculations of thermodynamic properties other than adsorption isotherms, such as solvation pressure [22;31;23].

Previously, the thermodynamic approach based on the DBdB theory was applied to the calculation of the solvation pressure in mesoporous materials with cylindrical pores only, such as SBA-15, porous glass, and templated monolithic silica, and demonstrated good agreement with models based on DFT [32] and experimental data [22;31;23]. Since the pore geometry has a large effect on the pressure inside the pore, due to the curvature that determines the strength of the adsorbate-wall interaction [10], there is a need to adapt this approach for the case of the spherical pore geometry.

In this work, we calculate solvation pressure induced by nitrogen in spherical silica mesopores using macroscopic DBdB theory, following the approach of Gor and Neimark [22], and compare it with the predictions by GCMC simulations. The results can be used for the prediction of the adsorption-induced deformation in mesoporous materials with spherical pore geometry, such as SBA-16 [33], FDU-1 [34], periodic mesoporous organosilicas [35;36], mesoporous silica thin films [37], and silica colloidal crystals [38;39].

METHODS

Molecular simulations are a powerful tool that can provide many insights on the thermodynamics of the fluid by means of statistical mechanics and is especially effective in the cases when thermodynamics of the system is different from one in the bulk case. In particular, the adsorption of gases in nanoconfinement can be calculated by GCMC simulation (at the constant chemical potential of the reservoir μ, the volume of the simulation cell V and temperature T). Molecular simulations, giving the atomistic description, leads to the best reproduction of the actual system without involving macroscopic approximations. However, for the large pores with a large number of adsorbing particles, the approach becomes computationally expensive and often non-feasible, leaving the room for DFT and macroscopic techniques. Here we give an overview of two methods for calculation of adsorption

isotherms: macroscopic DBdB theory [28] and microscopic GCMC simulations. We then proceed with the description of the calculation of solvation pressure in the spherical mesopores, from DBdB theory introduced earlier for the cylindrical pores [22], and from molecular simulations.

Derjaguin-Broekhoff-de Boer Theory

The adsorption isotherm is defined as the amount of gas or fluid adsorbed as a function of the gas (vapor) pressure p during an experiment (in a reservoir). At each of the points on adsorption isotherm the system is carefully equilibrated, so that the chemical potential μ of adsorbed fluid is the same as of the gas phase, which is typically estimated from the measured pressure assuming the ideal gas law

$$\mu = \mu_0 + k_{\mathrm{B}} T \ln(p/p_0), \tag{1}$$

where k_{B} is the Boltzmann constant, T is the absolute temperature, p is the vapor pressure and p_0 is the saturated vapor pressure at this temperature. In the further calculations, we put $\mu_0 = \mu(p_0) = 0$ for the sake of shortness. It is also assumed that the thermodynamic properties of the adsorbed fluid are similar to those of the bulk liquid.

According to DBdB theory [28;29] the chemical potential of the liquid film on the walls of spherical pore consists of two parts: a term related to the curvature of the liquid film and a term describing the interaction between the pore wall and the adsorbate. Thus, the chemical potential of the equilibrated system can be written as

$$\mu_{\mathrm{DBdB}} = -\left(\frac{2\gamma}{R-h} + \Pi(h)\right) v_{\mathrm{l}}, \tag{2}$$

where γ is the vapor-liquid surface tension, R is the radius of the pore, h is the liquid film thickness, v_{l} is the molecular volume of the adsorbed fluid, which is assumed to be the same as of the bulk liquid, and $\Pi(h)$ is the disjoining pressure as a function of h.

Eq. 2 decouples the effect of the film curvature (first term) and the effect of the solid-fluid interactions (second term) on the properties of the adsorbed film. The disjoining pressure Π depends only on the film thickness and assumed the same as if the fluid were adsorbed on the flat surface. Therefore, the parameters for $\Pi(h)$ are usually taken based on the reference data of the adsorption on the planar surface and often represented in the form of Frenkel-Halsey-Hill equation (FHH) [40;41;42]:

$$\Pi(h) = \frac{k_{\mathrm{B}} T}{v_{\mathrm{l}}} \frac{k}{(h/h_0)^m}, \tag{3}$$

where k and m are dimensionless parameters, $h_0 = 1$ Å. Another form of the disjoining pressure, widely used for describing adsorption on silica and glass surfaces [31;23;43], is

$$\Pi(h) = \Pi_0 \exp\left(-\frac{h}{\lambda}\right), \tag{4}$$

where Π_0 and λ are the parameters derived from experiments, which have the dimensions of pressure and length, respectively.

During adsorption process the capillary condensation takes place when the liquid film described by Eq. 2 loses its stability. The limiting film thickness h_{c} corresponding to the point of the condensation is found from the condition

$$\frac{\mathrm{d}\mu_{\mathrm{DBdB}}}{\mathrm{d}h} = 0, \tag{5}$$

which, using Eq. 2, gives

$$\left.\frac{\mathrm{d}\Pi(h)}{\mathrm{d}h}\right|_{h=h_\mathrm{c}} + \frac{2\gamma}{(R-h_\mathrm{c})^2} = 0. \tag{6}$$

The pressure at which capillary condensation occurs p_c can be found by substituting h_c into the Eq. 2 and Eq. 1.

Capillary evaporation during desorption process is determined by the equilibrium transition from a filled pore with a meniscus to a pore with a liquid film, which is given by the equality of the system free energy change zero, which results to [29]

$$k_\mathrm{B}T\ln(p_\mathrm{e}/p_0) = -3v_\mathrm{l}\left[\frac{\gamma}{R-h_\mathrm{e}} + \frac{1}{(R-h_\mathrm{e})^3}\int_{h_\mathrm{e}}^{R}(R-h')^2\Pi(h')\mathrm{d}h'\right]. \tag{7}$$

This equation combined with Eq. 2 provides the equilibrium film thickness corresponding to capillary evaporation, h_e, and the corresponding vapor pressure, p_e. Therefore, Eq. 6 and Eq. 7 for the critical and equilibrium values of h combined with Eq. 1 and Eq. 2 allow to fully predict the adsorption isotherm for the given pore size.

In this work, the macroscopic parameters taken for liquid nitrogen are γ = 8.88 mN/m, v_l = 34.66 cm^3/mol. The parameterization of DBdB model is done based on the disjoining pressure isotherm measured on reference (macroporous) silica material [38] using both forms of $\Pi(h)$. The results of the fitting are shown in Fig. 1. The disjoining pressure represented by Eq. 4 gives the remarkable agreement with the experimental data comparing to FHH isotherm, although the agreement with the adsorption isotherm is opposite in the regions of high pressure (Fig. 1b). Attempt to improve the agreement in the region of high pressure resulted in its deterioration in the region of low pressure. Since we focus here mostly on the adsorption-induced effects which take place in the thin film regions (before the capillary phase transitions), the accurate description of the adsorption at low pressure is more important for further consideration of the solvation pressure. Thus, we proceed with the exponential form of the disjoining pressure for the calculations based on the DBdB theory, i.e. Eq. 4. The parameters are summarized in Table 1.

Molecular Simulations

Monte Carlo simulation uses an atomistically detailed system and interactions between particles. In this work, the fluid-fluid interaction was represented by the Lennard-Jones potential. The interaction between silica pore walls and adsorbate is represented as an effective potential of the interaction between the oxygen atoms and the gas molecules [44]:

$$\begin{aligned} U_\mathrm{sf}(r,R) &= 2\pi n_\mathrm{s}\epsilon_\mathrm{sf}\sigma_\mathrm{sf}^2 \\ &\times\left\{\frac{2}{5}\sum_{i=0}^{9}\left[\frac{\sigma_\mathrm{sf}^{10}}{R^i\,(R-r)^{10-i}} + \frac{\sigma_\mathrm{sf}^{10}}{R^i\,(R+r)^{10-i}}\right]\right. \\ &\left. -\sum_{i=0}^{3}\left[\frac{\sigma_\mathrm{sf}^{4}}{R^i\,(R-r)^{4-i}} + \frac{\sigma_\mathrm{sf}^{4}}{R^i\,(R+r)^{4-i}}\right]\right\}, \end{aligned} \tag{8}$$

where n_s is the surface number density of solid atoms, σ_sf and ϵ_sf are the distance corresponding to zero potential and the potential well depth of the Lennard-Jones potential, respectively, r is the distance from the center of the pore, and R is the radius of the pore corresponding to the "external" diameter d_ext, the distance between the centers of the furthest solid atoms. The "internal" diameter, corresponding to the volume V used for the calculation of the adsorption amount, is related to the external diameter d_ext as [45]: $d_\mathrm{int} \approx d_\mathrm{ext} - 1.7168\sigma_\mathrm{sf} + \sigma_\mathrm{ff}$, where σ_ff is the Lennard-Jones radius for fluid-fluid interaction. The potentials were truncated at $r_\mathrm{cut} = 5\sigma_\mathrm{ff}$ and no tail corrections were used.

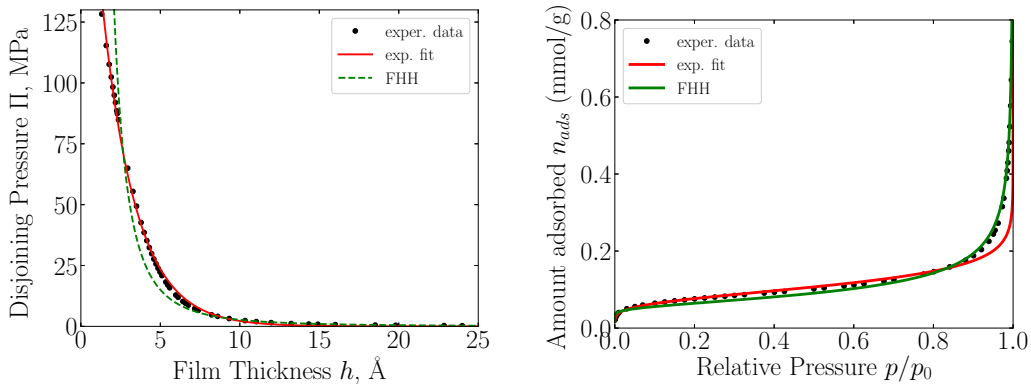

(a) **(b)**

FIGURE 1 Comparison of the fitting of the experimental isotherm of nitrogen adsorption on reference silica material[38] using DBdB theory with different forms of the disjoining pressure. Obtained parameters for Eq. 3 are k = 47.17 and m = 2.53 and for Eq. 4 are Π_0 = 251 MPa and λ = 2.10. For further calculations, the disjoining pressure was chosen to be represented by Eq. 4.

In the GCMC method, the pores were modeled with the external diameters ranging from 2 to 10 nm. Simulations were conducted for each the integer pore sizes and 4.5 nm for at least 10^{10} trial moves, third of which was used for calculation of the ensemble averages. For the rest of the pore sizes, 10^9 moves were used. The calculations of adsorption isotherms were done for nitrogen sorption at the normal boiling temperature of 77.4 K for the set of silica pores of different sizes. The reference chemical potential (at saturation point) was determined using the equation of state by Johnson et al.[46]. Parameters of the silica - nitrogen system used in the calculations are summarized in Table 1.

TABLE 1 Microscopic parameters for the N_2-N_2 fluid-fluid (ff) and SiO_2-N_2 solid-fluid (sf) interactions[45], and disjoining pressure parameters for SiO_2-N_2 at 77.4 K determined based on experimental data from Ref. 38.

	σ, nm	ϵ/k_B, K	n_s, nm^{-2}	Π_0, MPa	λ, Å
N_2-N_2	0.36154	101.5			
SiO_2-N_2	0.317	147.3	15.3	251.0 ± 3.1	2.11 ± 0.03

Solvation Pressure Calculation

Following the derivations given in Ref. 22 for the solvation pressure in cylindrical mesopores, we perform similar calculations for the case of the spherical geometry. Therefore, the solvation pressure can be determined by the derivative of the grand thermodynamic potential Ω of the adsorbed phase with respect to the volume:

$$P_{\mathrm{s}} = -\frac{1}{4\pi R^2}\left(\frac{\partial \Omega}{\partial R}\right)_{\mu,T}. \tag{9}$$

Note that for adsorption at subcritical conditions $P_{\mathrm{s}} \gg p$ and we thus neglect the terms with p explicitly written in Ref. 22. For the film region, the equation for solvation pressure can be obtained from

$$\Omega^{\mathrm{f}}(p) = \Omega(0) - \int_{-\infty}^{\mu(p)} N^{\mathrm{f}}(\mu')\mathrm{d}\mu', \tag{10}$$

where N^{f} is the amount of gas adsorbed, $\Omega(0) = 4\pi R^2\gamma_{\mathrm{s}}$ is the grand thermodynamic potential of the dry pore and γ_{s} is the surface tension of the dry solid. The amount of gas adsorbed is

$$N^{\mathrm{f}} = \frac{4\pi}{3v_{\mathrm{l}}}[R^3 - (R-h)^3], \tag{11}$$

where $h = h(\mu) = h(p)$. Therefore, following Eq. 10 and Eq. 2 the solvation pressure in the film region is determined as (the details of the derivation can be found in the Supplementary Material)

$$P_{\mathrm{s}}^{\mathrm{f}}(p) = -\frac{2\gamma_{\mathrm{s}}}{R} + \frac{2\gamma}{R} - \frac{2\gamma}{R-h} - \frac{2h}{R}\Pi(h) + \frac{h^2}{R^2}\Pi(h) + \frac{2}{R}\int_0^h \Pi(h')\mathrm{d}h' - \frac{2}{R^2}\int_0^h h'\Pi(h')\mathrm{d}h'. \tag{12}$$

Representing the disjoining pressure in the form of Eq. 4, Eq. 12 can be written as:

$$P_{\mathrm{s}}^{\mathrm{f}}(p) = -\frac{2\gamma_{\mathrm{s}}}{R} + \frac{2\gamma}{R} - \frac{2\gamma}{R-h} - \frac{\Pi_0 h}{R}\exp\left(-\frac{h}{\lambda}\right)\left(2 - \frac{h}{R}\right) + \frac{2\Pi_0}{R}\left[\lambda - \lambda\exp\left(-\frac{h}{\lambda}\right)\right] - \frac{2\Pi_0\lambda}{R^2}\left[\lambda - \exp\left(-\frac{h}{\lambda}\right)(h+\lambda)\right]. \tag{13}$$

Solvation pressure in a pore after the capillary condensation is written as

$$P_{\mathrm{s}}(p)_{\mathrm{filled}} = -\frac{2\gamma_{\mathrm{sl}}}{R} + \frac{R_{\mathrm{g}}T}{v_{\mathrm{l}}}\ln\left(\frac{p}{p_0}\right), \tag{14}$$

where the second term is the Laplace pressure. Value of γ_{sl} can be obtained from the Frumkin-Derjaguin equation[47] written for the case of the spherical pore:

$$\gamma_{\mathrm{sl}} = \gamma_{\mathrm{s}} - \frac{1}{R^2}\int_0^R (R-h)^2\Pi(h)\mathrm{d}h - \frac{2\gamma}{R^2}\int_0^R (R-h)\mathrm{d}h, \tag{15}$$

or, with the disjoining pressure in the form of Eq. 4,

$$\gamma_{\mathrm{sl}} = \gamma_{\mathrm{s}} - \gamma - \frac{2\Pi_0\lambda^2}{R}\left[\frac{R}{2\lambda} + \frac{\lambda}{R}\left(1 - \exp\left(-\frac{R}{\lambda}\right)\right) - 1\right]. \tag{16}$$

Therefore, Eq. 14 takes the form:

$$P_{\mathrm{s}}(p)_{\mathrm{filled}} = -\frac{2\gamma_{\mathrm{s}}}{R} + \frac{2\gamma}{R} + \frac{4\Pi_0\lambda^2}{R^2}\left[\frac{R}{2\lambda} + \frac{\lambda}{R}\left(1 - \exp\left(-\frac{R}{\lambda}\right)\right) - 1\right] + \frac{R_{\mathrm{g}}T}{v_{\mathrm{l}}}\ln\left(\frac{p}{p_0}\right). \tag{17}$$

The solvation pressure can thus be calculated by DBdB theory using Eq. 13 and Eq. 14.

Another approach is to use the molecular simulations, i.e., to calculate the amount adsorbed according to the method described in the Methods section. Given an adsorption isotherm, the grand thermodynamic potential of the adsorbed fluid can be extracted from Eq. 10. Following Eq. 9, the solvation pressure thus can be obtained by calculating the difference in the grand potential between isotherms obtained from GCMC simulations with the small variation of the pore size [17;8]. Eq. 9 gives the following discrete form:

$$P_{\mathrm{s}}(\mu, R) = -\frac{1}{4\pi R^2}\frac{\Omega(\mu, R + \Delta R) - \Omega(\mu, R - \Delta R)}{2\Delta R}, \tag{18}$$

where ΔR is the shift from the pore size R. Pore sizes $R + \Delta R$ and $R - \Delta R$ should have close values or, alternatively, the chemical potential mesh should have enough precision so that for each distinct chemical potential, all points corresponding to these pore sizes in the band should lie either before or after the point of capillary condensation. In our case, to satisfy this criterion, we chose pore size increment ΔR as 0.05 nm and chemical potential mesh with 21 points equidistantly located in the relative pressure space within the 0 to 1 interval. Additionally, we applied high-order finite difference approximation with five points, and it gave consistent results with the two-point formula. The comparison plot is available in Supplementary Material.

RESULTS

Adsorption Isotherms

The calculations of the isotherms of nitrogen adsorption on silica using DBdB theory were performed according to the Methods section. The internal pore diameters used in DBdB equations were recalculated from the external diameters in the range of 2-10 nm, the difference is explained in details in Ref. 48. Comparison of the isotherms is shown in Fig. 2. Here and further the label shows the corresponding external diameters. DBdB approach provides a reasonably good description of simulated isotherms, which deteriorates as pore size decreases, which is expected for the macroscopic theory. For the isotherms predicted by DBdB we show the equilibrium desorption branch, however, it is unlikely that experimental desorption branch would go along that path, as a system of necks connecting the pores typically lead to pore blocking or cavitation mechanisms of desorption [49;50].

Solvation Pressure

The solvation pressure in a spherical pore is calculated by DBdB theory using Eq. 9 and Eq. 14, shifted by $\frac{2\gamma_{\mathrm{s}}}{R}$, in order to satisfy the condition of zero solvation pressure in the dry pore. Calculations by GCMC simulations were done using Eq. 18 and the comparison of results obtained by the two approaches is shown in Fig. 3. Both theories show the trend typical for the solvation pressure caused by adsorption in mesopores: gradual increase following by sharp decrease at the point of the capillary

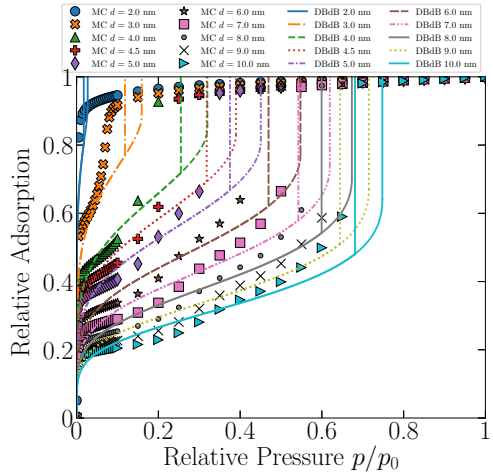

FIGURE 2 Adsorption isotherms for nitrogen at 77.4 K in spherical silica pores of different sizes, predicted by DBdB (lines) and GCMC (markers). Relative adsorption is defined as a ratio of the volume of the pore when it is filled with adsorbate to the total pore volume.

condensation, and DBdB additionally shows the opposite behavior on the desorption path. The obtained curves diverge only slightly, with the result from DBdB shifted toward lower pressures.

Fig. 4 shows the dependence of the solvation pressure on the pore size at the saturated vapor pressure. For the pore of 4 nm and above the dependence is linear, but below that the linear trend deteriorates, i.e. when the pore size approaches the limit of the mesoporous region[26]. Based on the relation given by Eq. 14, noting that the intercept is close to zero as the pore size goes to infinity, application of the linear fit in the region of 4-10 nm allows one to get the value $\gamma_{\mathrm{s}} - \gamma_{\mathrm{sl}} = 66 \pm 0.1$ mN/m. Fig. 5 shows the comparison between GCMC prediction and DBdB prediction recalculated with the obtained value of $\gamma_{\mathrm{s}} - \gamma_{\mathrm{sl}}$. The resulted agreement is remarkable both qualitatively and quantitatively for the pores larger than 3 nm and in particular is excellent for the pore sizes of 6-10 nm, except the points of the capillary transitions, which was also the case for the adsorption isotherms. Moreover, the predicted mechanism of the deformation became different: sharp decrease of the solvation pressure has changed to the sharp increase with the opposite behavior on the desorption path.

DISCUSSION

We employed macroscopic DBdB theory for the calculation of the solvation pressure in spherical mesopores and compared results with molecular simulations, which has not been previously done. First of all, we showed the comparison of the adsorption isotherms and revealed a slight quantitative deviation between the approaches. The reason is mainly in the representation of the solid-fluid interaction by the DBdB theory: it assumes that the disjoining pressure depends only on the thickness of the adsorbed liquid film, but not the radius of curvature of the pore and is taken the same as for planar surface. Moreover, the obtained two-parametric fit of the experimental isotherm with the disjoining pressure curve is not quite rigorous, introducing additional

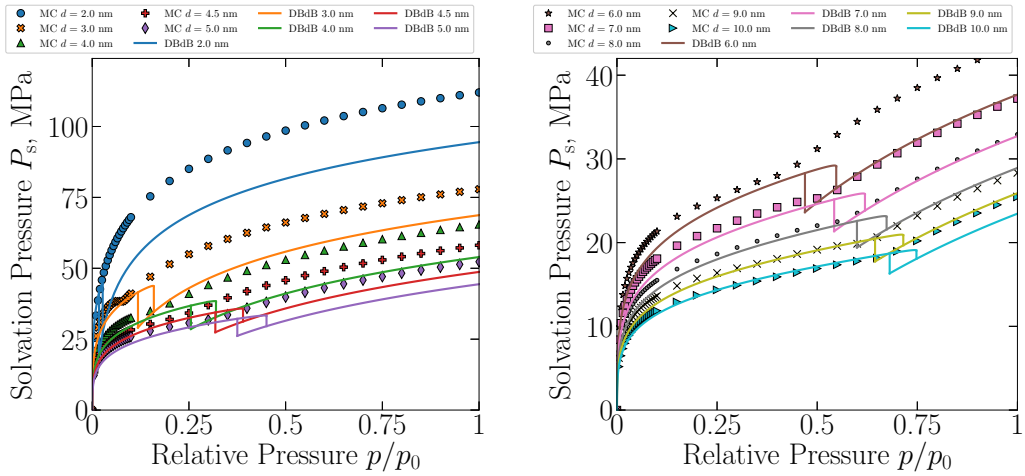

(a) **(b)**

FIGURE 3 Solvation pressure for nitrogen adsorbed at 77.4 K in spherical silica pores of 2-5 nm sizes (a) and 6-10 nm sizes (b). Solid lines represent the calculations based on macroscopic approach and markers based on GCMC simulations.

error to the description by DBdB theory. Although the other forms of the disjoining pressure isotherm, such as FHH, can be employed for the calculation of the adsorption isotherms, it is not suitable for the calculation of the solvation pressure, due to the discontinuity at the zero film thickness, shown in Ref. 22.

Solvation pressure curves, calculated by two methods, are consistent with each other, and typical for the solvation pressure in mesoporous materials, yet noticeably differ from the results for cylindrical pore geometry [22]. The difference is seen at the capillary condensation points: the solvation pressure calculated here shows a slight increase during the capillary condensation, while in the cylindrical pores, the decrease was observed [22]. The dependence of the solvation pressure at the saturation on the reciprocal pore size, predicted by GCMC results, first of all, shows a strict linear dependence, secondly, it allows to extract the change of solid surface energy due to adsorption. The solvation pressure recalculated by DBdB theory with the obtained value gave a remarkable agreement between two approaches. This agreement suggests that the initial noticeable discrepancy between DBdB and GCMC in the region after the capillary condensation is due to the approximate Frumkin-Derjaguin equation, employed for the calculation of solid-liquid surface energy. The Frumkin-Derjaguin equation introduces imprecision through the inaccuracy of the disjoining pressure isotherm in the limit of dry surface. Overall, the achieved consistency between theories suggests the usage of both approaches combined for the prediction of solvation pressure: when molecular simulations become expensive, i.e. for the large pore sizes, the DBdB theory is a reliable alternative.

Moreover, both methods captured the difference in the trend of the solvation pressure in spherical and cylindrical pores, showing the correspondence to the expansion of the pore during the capillary condensation transition, instead of contraction, observed for the deformation in the most of the experimental and simulated systems [1]. These results can be applied for predicting adsorption-induced deformation of mesoporous materials with the pores, which are modeled as spherical, such as SBA-16 silica, mesoporous organosilica, and synthetic opals.

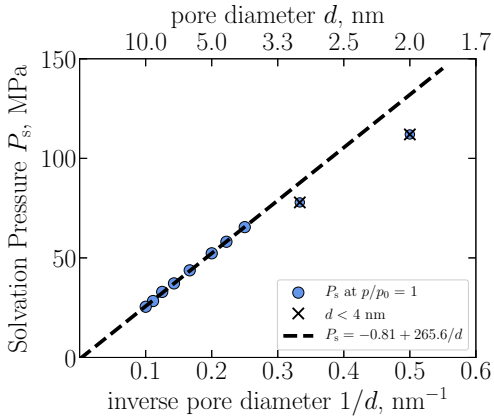

FIGURE 4 Solvation pressure for nitrogen adsorbed at 77.4 K in spherical silica pores of various sizes calculated using GCMC at the saturation pressure ($p = p_0$), plotted as a function of reciprocal pore diameter. Markers show the data, and the dashed line shows the linear fit for pores 4 nm and larger. The crossed markers indicate the points not used in the linear fit.

CONCLUSION

We presented a theoretical study on the high pressure effect in the nanopores. We specifically focused on adsorption of nitrogen at its normal boiling point in spherical silica mesopores. We calculated the solvation pressure, i.e. the normal component of the pressure tensor in the fluid, which is the driving force for the adsorption-induced deformation. The calculations were done using two different methods: the macroscopic DBdB theory and GCMC. The results for the two methods showed excellent agreement; they are also similar to the published results on the solvation pressure in the pores with the cylindrical geometry. This suggests the applicability of the presented results for predicting solvation pressure and adsorption-induced deformation of silica materials with spherical pores.

REFERENCES

1. Gor GY, Huber P, Bernstein N. Adsorption-induced deformation of nanoporous materials – A review. *Appl. Phys. Rev.* 2017; 4(1): 011303.

2. Kaneko K, Fukuzaki N, Kakei K, Suzuki T, Ozeki S. Enhancement of nitric oxide dimerization by micropore fields of activated carbon fibers. *Langmuir* 1989; 5(4): 960–965.

3. Byl O, Kondratyuk P, Yates J. Adsorption and dimerization of NO inside single-walled carbon nanotubes an infrared spectroscopic study. *J. Phys. Chem. B* 2003; 107(18): 4277–4279.

4. Schappert K, Pelster R. Influence of the Laplace pressure on the elasticity of argon in nanopores. *Europhys. Lett.* 2014; 105(5): 56001.

5. Gor GY. Adsorption Stress Changes the Elasticity of Liquid Argon Confined in a Nanopore. *Langmuir* 2014; 30(45): 13564–13569.

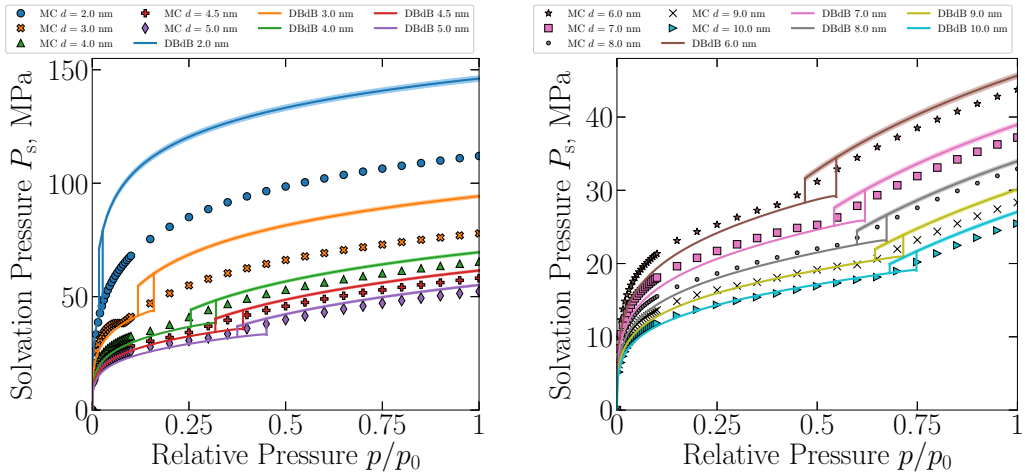

(a) **(b)**

FIGURE 5 Solvation pressure for nitrogen adsorbed at 77.4 K in spherical silica pores of 2-5 nm sizes (a) and 6-10 nm sizes (b), the value of $\gamma_s - \gamma_{sl}$ is calculated from Fig. 4, with the shaded region representing the error. Solid lines represent the calculations based on macroscopic approach and markers based on GCMC simulations.

6. Gor GY, Siderius DW, Shen VK, Bernstein N. Modulus–Pressure Equation for Confined Fluids. *J. Chem. Phys.* 2016; 145(16): 164505.

7. Maximov MA, Gor GY. Molecular simulations shed light on potential uses of ultrasound in nitrogen adsorption experiments. *Langmuir* 2018; 34(51): 15650–15657.

8. Long Y, Palmer JC, Coasne B, Śliwinska-Bartkowiak M, Gubbins KE. Pressure enhancement in carbon nanopores: a major confinement effect. *Phys. Chem. Chem. Phys.* 2011; 13(38): 17163–17170.

9. Long Y, Palmer JC, Coasne B, Śliwinska-Bartkowiak M, Gubbins KE. Under pressure: Quasi-high pressure effects in nanopores. *Micropor. Mesopor. Mat.* 2012; 154: 19–23.

10. Long Y, Śliwińska-Bartkowiak M, Drozdowski H, et al. High pressure effect in nanoporous carbon materials: effects of pore geometry. *Colloids Surf. A* 2013; 437: 33–41.

11. Long Y, Palmer JC, Coasne B, et al. On the molecular origin of high-pressure effects in nanoconfinement: The role of surface chemistry and roughness. *J. Chem. Phys.* 2013; 139(14): 144701.

12. Coasne B, Long Y, Gubbins K. Pressure effects in confined nanophases. *Mol. Simul.* 2014; 40(7-9): 721–730.

13. Gubbins KE, Long Y, Śliwinska-Bartkowiak M. Thermodynamics of confined nano-phases. *The Journal of Chemical Thermodynamics* 2014; 74: 169–183.

14. Srivastava D, Santiso EE, Gubbins KE. Pressure enhancement in confined fluids: effect of molecular shape and fluid–wall interactions. *Langmuir* 2017; 33(42): 11231–11245.

15. Addington CK, Long Y, Gubbins KE. The pressure in interfaces having cylindrical geometry. *J. Chem. Phys.* 2018; 149(8): 084109.

16. Balbuena PB, Berry D, Gubbins KE. Solvation pressures for simple fluids in micropores. *J. Phys. Chem.* 1993; 97(4): 937–943.

17. Ravikovitch PI, Neimark AV. Density functional theory model of adsorption on amorphous and microporous silica materials. *Langmuir* 2006; 22(26): 11171–11179.

18. Kowalczyk P, Ciach A, Neimark AV. Adsorption-induced deformation of microporous carbons: Pore size distribution effect. *Langmuir* 2008; 24(13): 6603–6608.

19. Do D, Nicholson D, Do H. Effects of adsorbent deformation on the adsorption of gases in slitlike graphitic pores: A computer simulation study. *J. Phys. Chem. C* 2008; 112(36): 14075–14089.

20. Yang K, Lu X, Lin Y, Neimark AV. Deformation of coal induced by methane adsorption at geological conditions. *Energy & Fuels* 2010; 24(11): 5955–5964.

21. Zeng Y, Liu L, Zhang H, Do D, Nicholson D. A Monte Carlo study of adsorption-induced deformation in wedge-shaped graphitic micropores. *Chem. Eng. J.* 2018; 346: 672–681.

22. Gor GY, Neimark AV. Adsorption-Induced Deformation of Mesoporous Solids. *Langmuir* 2010; 26(16): 13021-13027.

23. Balzer C, Waag AM, Gehret S, et al. Adsorption-induced deformation of hierarchically-structured mesoporous silica – effect of local anisotropy. *Langmuir* 2017; 33(22): 5592-5602.

24. Gubbins KE, Liu YC, Moore JD, Palmer JC. The role of molecular modeling in confined systems: impact and prospects. *Phys. Chem. Chem. Phys.* 2011; 13(1): 58–85.

25. Landers J, Gor GY, Neimark AV. Density Functional Theory Methods for Characterization of Porous Materials. *Colloids Surf., A* 2013; 437: 3–32.

26. Thommes M, Kaneko K, Neimark AV, et al. Physisorption of gases, with special reference to the evaluation of surface area and pore size distribution (IUPAC Technical Report). *Pure Appl. Chem.* 2015; 87(9-10): 1051–1069.

27. Derjaguin BV. A theory of capillary condensation in the pores of sorbents and of other capillary phenomena taking into account the disjoining action of polymolecular liquid films. *Acta Physicochim. URSS* 1940; 12: 181 - 200.

28. Broekhoff JCP, De Boer JH. Studies on pore systems in catalysts: IX. Calculation of pore distributions from the adsorption branch of nitrogen sorption isotherms in the case of open cylindrical pores A. Fundamental equations. *J. Catal.* 1967; 9(1): 8–14.

29. Broekhoff JCP, De Boer JH. Studies on pore systems in catalysts: XI. Pore distribution calculations from the adsorption branch of a nitrogen adsorption isotherm in the case of "ink-bottle" type pores. *J. Catal.* 1968; 10(2): 153–165.

30. Neimark AV, Ravikovitch PI. Capillary condensation in MMS and pore structure characterization. *Micropor. Mesopor. Mat.* 2001; 44-45: 697 - 707.

31. Gor GY, Paris O, Prass J, Russo PA, Ribeiro Carrott MML, Neimark AV. Adsorption of n-Pentane on Mesoporous Silica and Adsorbent Deformation. *Langmuir* 2013; 29(27): 8601–8608.

32. Gor GY, Neimark AV. Adsorption-induced deformation of mesoporous solids: Macroscopic approach and density functional theory. *Langmuir* 2011; 27(11): 6926–6931.

33. Zhao D, Huo Q, Feng J, Chmelka BF, Stucky GD. Nonionic triblock and star diblock copolymer and oligomeric surfactant syntheses of highly ordered, hydrothermally stable, mesoporous silica structures. *J. Am. Chem. Soc.* 1998; 120(24): 6024–6036.

34. Matos JR, Kruk M, Mercuri LP, et al. Ordered mesoporous silica with large cage-like pores: structural identification and pore connectivity design by controlling the synthesis temperature and time. *J. Am. Chem. Soc.* 2003; 125(3): 821–829.

35. Burleigh MC, Markowitz MA, Spector MS, Gaber BP. Direct synthesis of periodic mesoporous organosilicas: functional incorporation by co-condensation with organosilanes. *J. Phys. Chem. B* 2001; 105(41): 9935–9942.

36. Matos JR, Kruk M, Mercuri LP, et al. Periodic mesoporous organosilica with large cagelike pores. *Chem. Mater.* 2002; 14(5): 1903–1905.

37. Yu K, Smarsly B, Brinker CJ. Self-Assembly and Characterization of Mesostructured Silica Films with a 3D Arrangement of Isolated Spherical Mesopores. *Adv. Funct. Mater.* 2003; 13(1): 47–52.

38. Galukhin A, Bolmatenkov D, Emelianova A, Zharov I, Gor GY. Porous Structure of Silica Colloidal Crystals. *Langmuir* 2019; 35(6): 2230–2235.

39. Maximov MA, Galukhin AV, Gor GY. Pore-Size Distribution of Silica Colloidal Crystals from Nitrogen Adsorption Isotherms. *Langmuir* 2019; 35(47): 14975–14982.

40. Frenkel JI. *Kinetic Theory of Liquids*. London: Oxford University Press . 1946.

41. Halsey G. Physical Adsorption on Non-Uniform Surfaces. *J. Chem. Phys.* 1948; 16(10): 931-937.

42. Hill TL, Frankenburg WG, Komarewsky VI, Rideal EK. *Theory of Physical Adsorption*. 4. Academic Press: New York . 1952.

43. Kolesnikov A, Georgi N, Budkov YA, et al. Effects of Enhanced Flexibility and Pore Size Distribution on Adsorption-Induced Deformation of Mesoporous Materials. *Langmuir* 2018; 34(25): 7575–7584.

44. Baksh MSA, Yang RT. Model for spherical cavity radii and potential functions of sorbates in zeolites. *AIChE J.* 1991; 37(6): 923–930.

45. Gor GY, Rasmussen CJ, Neimark AV. Capillary Condensation Hysteresis in Overlapping Spherical Pores: A Monte Carlo Simulation Study. *Langmuir* 2012; 28(33): 12100–12107.

46. Johnson JK, Zollweg JA, Gubbins KE. The Lennard-Jones equation of state revisited. *Mol. Phys.* 1993; 78(3): 591–618.

47. Rusanov AI. On the Thermodynamics of Thin Films. The Frumkin–Derjaguin Equation. *Colloid J.* 2020; 82(1): 62–68.

48. Dobrzanski CD, Maximov MA, Gor GY. Effect of pore geometry on the compressibility of a confined simple fluid. *J. Chem. Phys.* 2018; 148(5): 054503.

49. Klomkliang N, Do D, Nicholson D. Effects of temperature, pore dimensions and adsorbate on the transition from pore blocking to cavitation in an ink-bottle pore. *Chem. Eng. J.* 2014; 239: 274–283.

50. Klomkliang N, Do DD, Nicholson D. Scanning curves in wedge pore with the wide end closed: Effects of temperature. *AIChE J.* 2015; 61(11): 3936–3943.